Vol 18 No 5, May 2009
1674-1056/2009/18(05)/1801-06

Chinese Physics B

© 2009 Chin. Phys. Soc.
and IOP Publishing Ltd

Terahertz radiation from armchair carbon nanotube dipole antenna*

Wang Yue(王 玥)[a)b)], Wu Qun(吴 群)[a)†], He Xun-Jun(贺训军)[b)],
Zhang Shao-Qing(张少卿)[a)], and Zhuang Lei-Lei(庄蕾蕾)[b)]

[a)] *School of Electronics and Information Technology, Harbin Institute of Technology, Harbin* 150001, *China*

[b)] *Department of Electrical Science and Technology, Harbin University of Science and Technology, Harbin* 150080, *China*

(Received 8 October 2008; revised manuscript received 6 November 2008)

This paper investigates the electromagnetic radiation characteristics of a metallic, large aspect ratio single walled carbon nanotube antenna in the terahertz frequency region below 12.5 THz. The key features of terahertz pulse have been revealed on the carbon nanotube antenna in comparison with conventional photoconductive switching. The terahertz waveforms, radiation power and their field distributions have been evaluated and are analysed. The Fourier transformed spectra over the whole frequency range demonstrate that the carbon nanotube antenna can be used as radiation source for broadband terahertz applications.

Keywords: terahertz, carbon nanotube, antenna
PACC: 0762, 7865, 4110H

1. Introduction

Terahertz (THz) waves (frequency interval from 0.1 to 10 THz), occupying a large portion of the electromagnetic spectrum between the infrared and microwave bands, are the next frontier in science and technology fields such as radar and microwave communications, far-infrared nonlinear optics, coherent control of materials, and generation of THz pulse trains.[1,2]

The generation of THz radiation by optical rectification or photoconductive switching has been extensively studied by using femtosecond (fs) laser pulses.[3−7]

Of these different methods, photoconductive switching generating THz emission has been proved to be a crucial and fundamental technique, and has been widely used for THz imaging and detecting. However, compared with relatively well-developed technologies at microwave and optical frequencies, basic research, new initiatives and advanced technology developments in the THz band are very limited. The THz band is a scientifically rich but technologically limited frequency band, because THz wave emitters and receivers are less developed, in comparison with its neighbouring bands (microwave and optical).

Since they were first discovered in 1991, carbon nanotubes (CNTs) have attracted much attention of scientists and engineers due to their unique physical, topological and mechanical properties. Especially, the outstanding electrical properties of CNTs offer the possibilities of using them in diverse applications ranging from nanoelectronic devices to chemical and biochemical sensors.[7−9] In recent years, there has been considerable interest in the optical properties of CNTs, which partly are ascribed to its particular configuration. As illustrated in Fig.1, a single-walled carbon nanotube (SWCN) can be regarded as a seamless cylinder consisting of a sheet of graphite rolled up into a tube having a radius of a few nanometres and length up to centimetres, and then multi-walled carbon nanotubes (MWCNs) are made by SWCNs nested concentrically inside one another. Experiments and theories have shown that CNTs can be either metallic with excellent conductivity or semiconducting with a band gap inversely proportional to the diameter of the tube, depending on the different chirality of the nanotube. In the metallic conductive mode, nanotubes have extremely low electrical resistance and are believed to conduct through ballistic transport. The benefit of ballistic transport is that the resistance of the tube is independent of its length. Because of their non-ohmic

*Project supported by the National Natural Science Foundation of China (Grant No 60571026) and the Science and Technology Research Foundation of Heilongjiang Education Bureau of China (Grant No 11531055).

†Corresponding author. E-mail: qwu@hit.edu.cn

properties and high thermal stability, nanotubes have an estimated current-carrying capacity of one billion Amperes per square centimetre, about one thousand times greater than copper wire.

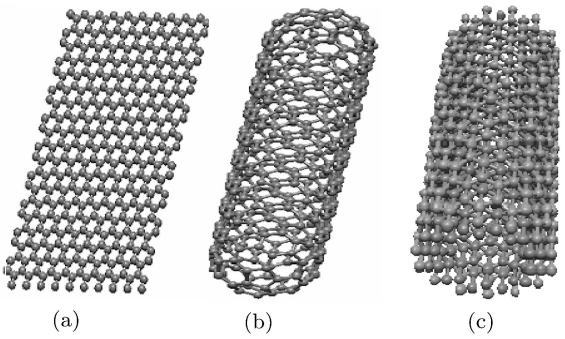


Fig.1. CNT is made of single graphite sheets. (a) A sheet of graphite, (b) SWCN, (c) MWCN.

Based on the outstanding metallic of CNTs and quasi-one-dimensional ballistic transportation of electron in CNTs, the visible and infrared antenna of CNTs have been studied both experimentally and theoretically, and have been shown to be an effective nanoantenna.[10−15] In their studies, both the polarization effect and the antenna effect have been demonstrated, and the characteristics of armchair CNTs are actively discussed in the infrared and optical region. However, their THz radiation properties have not been investigated thoroughly.[16] To complete the preliminary THz wave antenna studies, it is useful to perform computer simulations of the detailed antenna radiation properties in the terahertz range.

In this study, we characterize the electromagnetic radiation properties of SWCN antenna in the THz frequency region below 12.5 THz and observe the waveform of the field of THz radiation using computer simulation technology microwave studio. Our results showed that a significant portion of the THz wave was contributed from the SWCN, in comparison with the reports of THz waves from a photoconductive antenna or other THz wave generators.

2. Carbon nanotubes antenna and modelling

As in graphite, the bonding in CNTs is sp^2, with each atom joined to three neighbours. The tubes can therefore be considered as rolled up graphemic sheets. The structure of CNTs can be specified by vector $\boldsymbol{C}_\mathrm{h} = n\boldsymbol{a}_1 + m\boldsymbol{a}_2$, where n, m are integers and $\boldsymbol{a}_1, \boldsymbol{a}_2$ are lattice basis vectors. Thus CNTs can be characterized by the dual indexes n, m. The first two types, known as armchair ($n = m$) and zigzag ($n = 0$) CNTs, have a high degree of symmetry. The third class of tubes is chiral CNTs ($m \neq n > 0$) which in practice is the most common. Armchair CNTs are always metallic, and therefore attention here will be focused on armchair SWCNs. The radius of CNTs is given by

$$R = \frac{C_\mathrm{h}}{2\pi} = \frac{\sqrt{3}}{2\pi} a_{\mathrm{c-c}} \sqrt{n^2 + nm + m^2},$$

where $a_{\mathrm{c-c}} = 0.142$ nm is the interatomic distance in grapheme. The structure of the CNT antenna is shown in Fig.2. Figure 2 shows the construction of the antenna and its corresponding coordinates. The radius and total length of the antenna are R and L, respectively, and the gap between dipoles is d ($d \ll L$). Theoretically, a simple dipole thin antenna maximizes its response to a wavelength λ in condition of $L = m\lambda/2$, where m is a positive integer.

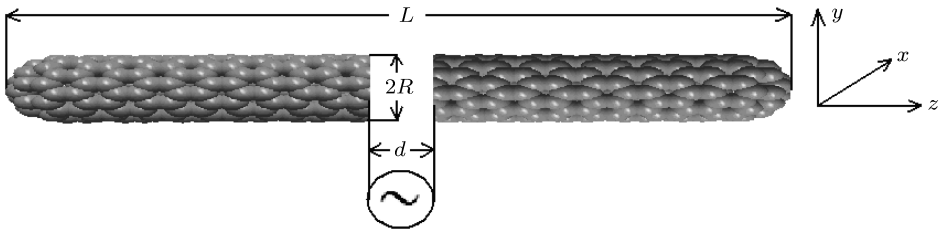


Fig.2. Structure of armchair SWCN antenna.

3. Results and discussions

Figure 3(a) shows a typical transient THz electric field waveform observed in the direction parallel to the dipole antenna with a length of $L = 0.5\lambda$ at $r = (5, 0, 0)$ μm. The first main positive and negative peaks of pulse have full width at half maxima of 59 fs and 56 fs, respectively. One can note that the THz pulse has a delay of about 164 fs, and that the THz signal shows several peaks corresponding to multiple THz reflections in the antenna. The maximum peak of the THz field is up to 2.66 kV/cm. Figure 3(b) shows a transient far field THz pulse in the direction at $r = (10, 0, 0)$ μm. Note that there is a delay of approximately 181 fs because of the propagation of the fields from the antenna edges to a probing point in the far field. The initial negative peak with a width of 56 fs is followed by a high peak pulse which persists for about 0.16 ps. As depicted in Fig.3(b), the maximum peak of THz field decreases to 1.26 kV/cm. Some weaker oscillations can be obviously seen for longer delays and the average oscillation period of the THz pulse is roughly 0.13 ps, which can result from current multiple reflections in the CNT antenna.

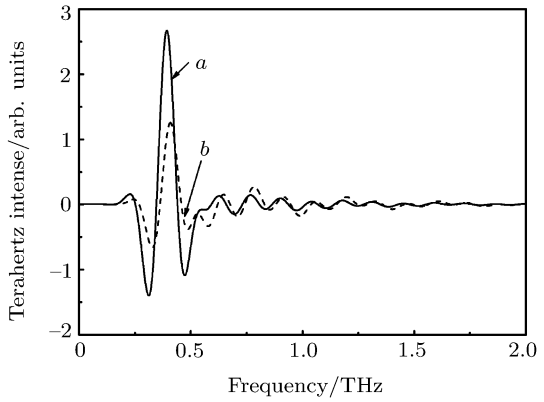


Fig.3. (curve a) THz pulse in a position to the parallel direction with the antenna of $L = 0.5\ \lambda$ at $r = (5, 0, 0)$ μm. (curve b) THz pulse at $r = (10, 0, 0)$ μm.

Figure 4 shows the Fourier transformed amplitude spectrum of the THz wave forms shown in Fig.3. From the figures it can be seen that the spectrum profiles are different for the two cases. The pulse width and antenna structure limit the Fourier transformed amplitude to about 12.5 THz. The spectra of THz pulses peak at roughly 5.3 THz and 5.0 THz for Figs.4(a) and 4(b), respectively. The spectral dips at 3.14 THz and 6.91 THz are observed (Fig.4(b)). The high frequency end of spectral distribution is extended to about 12.5 THz, which is less than the 30 THz reported so far for the photoconductor antenna. But such results imply another approach to generate THz radiation by the CNT antenna.

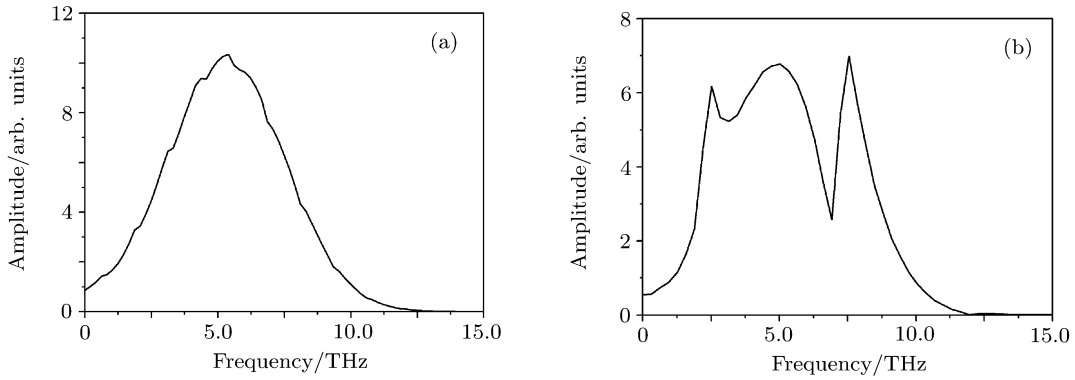


Fig.4. Fourier amplitude of the waveforms shown in Fig.3. (a) The corresponding frequency distributions calculated for the THz pulse in Fig.3(a). (b) The corresponding frequency distributions calculated for the THz pulse in Fig.3(b).

The output power spectra of THz wave are shown in Fig.5. The THz peak power observed from Fig.5(a) is up to 5 μW, and the THz peak power observed from Fig.5(b) is merely sixteen-hundredth of that observed from Fig.5(a). At very high frequency, the most of the generated THz power is lost during the travel along the free space due to dielectric loss and radiation loss, at the same time, the output power is influenced by the applied voltage, antenna pattern and mobility of the electrons. From Fig.5, it can be seen that the output power rapidly declines when the frequency is greater than 12.5 THz.

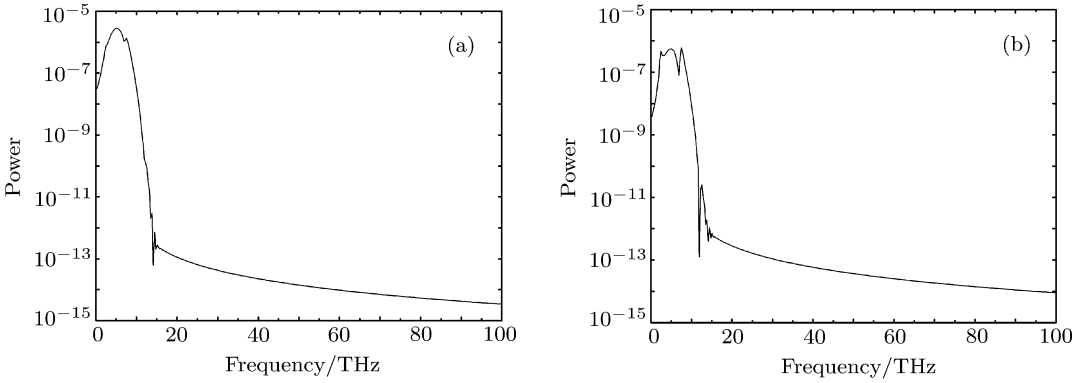


Fig.5. The output power of (a) THz pulse shown in Fig.3(a) and of (b) THz pulse shown in Fig.3(b).

Figure 6 shows the time domain wave form, Fourier transformed spectra, and the power spectra of the THz pulse obtained with CNT of $L = 1.5\lambda$ at different observed points. From Fig.6(a) it can be seen that the spectra of the THz pulse have no obvious oscillation, and the peaks of THz pulse decrease gradually with the increasing distance from observed point to the CNT antenna. The frequency distributions of the Fourier-transformed spectra (Fig.6(b)) extend to 11 THz. Figures 6(c) and 6(d) plot the spectra of the THz pulse as a function of frequency. The peak power dropped by an average of about 10% in comparison with the results of Fig.5. In the frequency greater than 15 THz, etalon oscillations are visible and are caused by multiple reflections in the CNT.

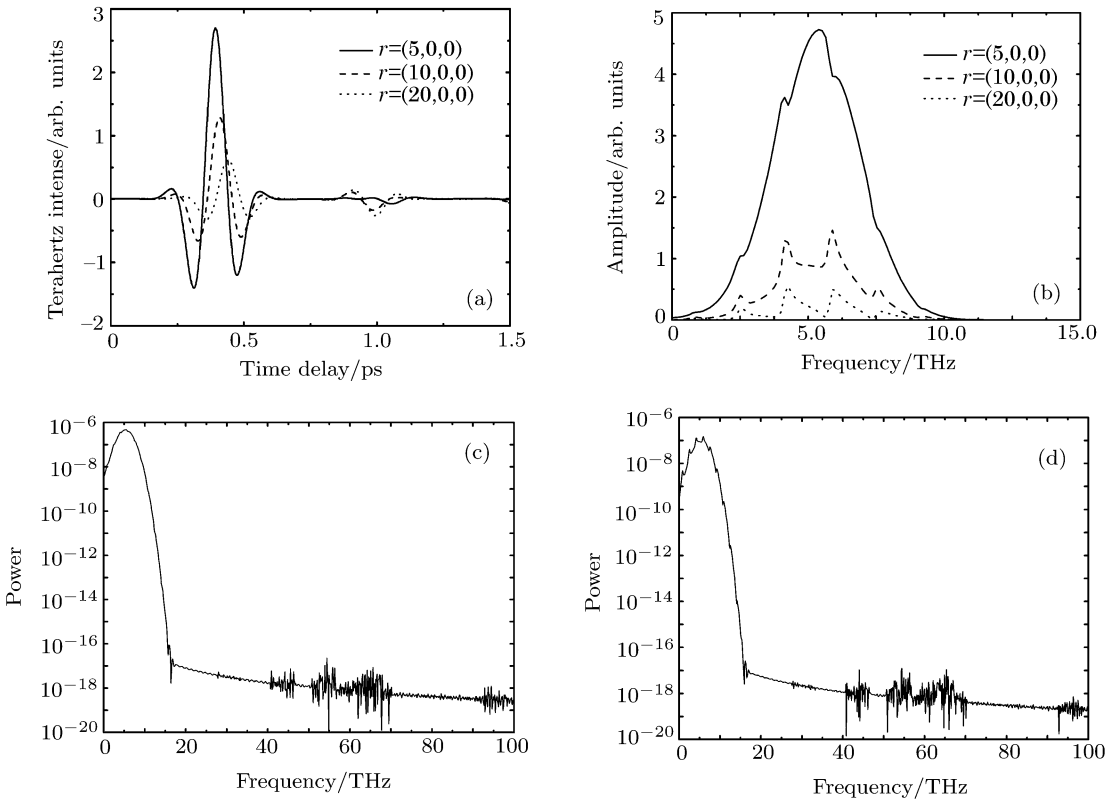


Fig.6. (a) THz time domain wave forms of the antenna of $L = 1.5\ \lambda$ at $r = (5, 0, 0)\ \mu$m(solid line), $r = (10, 0, 0)\ \mu$m (dashed line), and $r = (20, 0, 0)\ \mu$m (dotted line); (b) frequency domain wave forms after fast Fourier transformations; (c) the output power at $r = (5, 0, 0)\ \mu$m; (d) the output power at $r = (10, 0, 0)\ \mu$m.

Figure 7 shows the scattering parameter (S11) and voltage standing wave ratio (VSWR) as a function of frequency, where the first resonant frequency (2.47 THz) is approximately equal to 2.5 THz by the practical electrical length calculated when the S11 < -10 dB, and second resonant frequency is 7.38 THz. The VSWR is less than 1.5:1 on the operating frequency from 2.36 THz to 2.58 THz and from 7.27 THz to 7.5 THz, corresponding to S11 < -10 dB bandwidths of 8.9% and 3.1%.

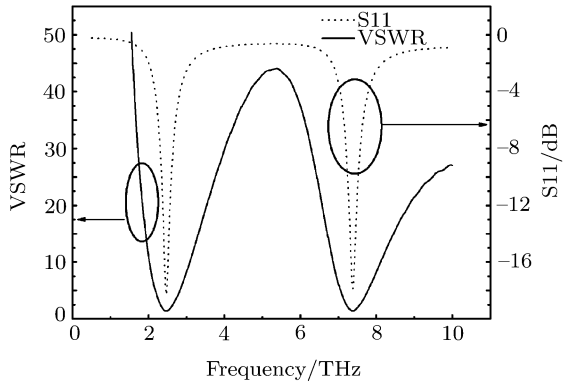


Fig.7. Scattering parameter and voltage standing wave ratio.

To highlight the THz radiation electric field production of CNT, we use the finite integration method to model spatial electric field distribution in the different directions at resonant frequencies of 2.47 THz and 7.38 THz, which are shown pictorially in Fig.8. As expected, strong THz fields are created within the antenna. The graphs on the left-hand side, middle, and right-hand side column, correspond to the planes $z = 30$ μm, $x = 30$ μm, and $y = 7$ μm, respectively. As can be recognized, there is a strong confinement effect on the surface of the CNT due to the plasmon oscillation that becomes increasingly pronounced for high frequencies. We note that although the THz field distributions are different, they are symmetric in all three directions. As can be seen from the Fig.8, the THz electric intensity in the higher frequency is stronger than that in the low frequency, and the periodic distributions of electric field are obtained in the high frequencies in Fig.8(e). The spatial patterns on the $x - z$ planes differ for various frequencies: the 2.47 THz frequency component propagates to the end of CNT in the z direction with a continuous attenuation, while the 7.38 THz component first decreases to zero, and then increases along the z direction. This suggests that the high frequency components of THz radiation are more easily generating oscillation.

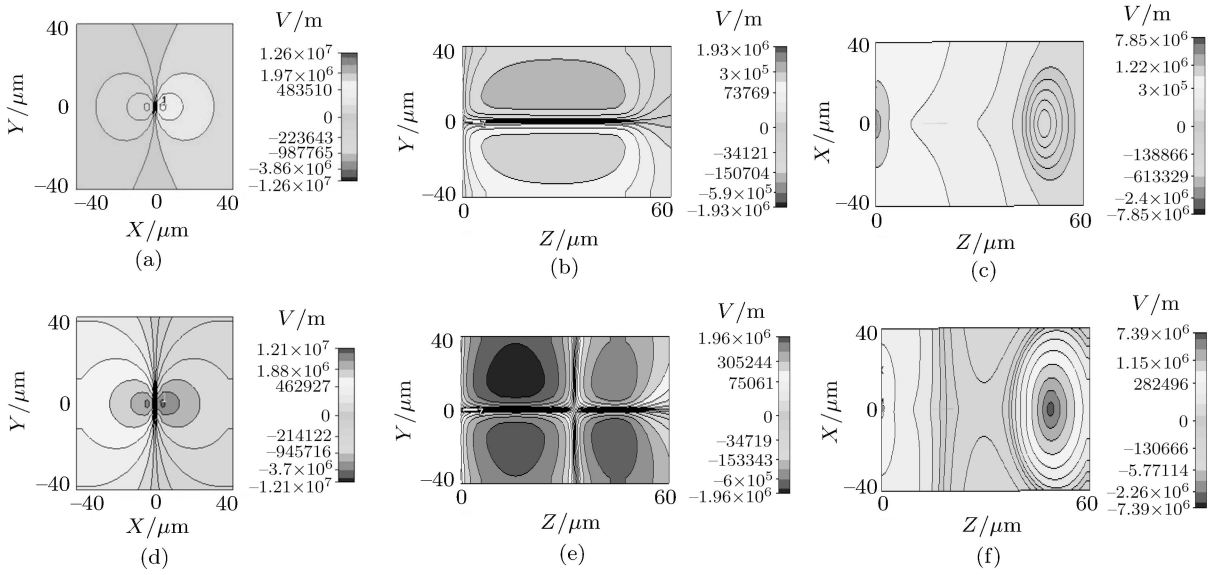


Fig.8. THz electric field distribution at various spatial planes. Graphs (a), (b), (c) and (d), (e), (f) are for the frequencies of 2.47 THz and 7.38 THz, respectively.

Figure 9 plots the radiation patterns for the CNT antenna at 2.47 THz and 7.38 THz. From the pictures, we can see that the maximum gains are 1.56 dBi and 3.73 dBi at 2.47 THz and 7.38 THz, respectively. In order

to increase the gain of the antenna, CNT arrays would be required and will be reported at a later date.

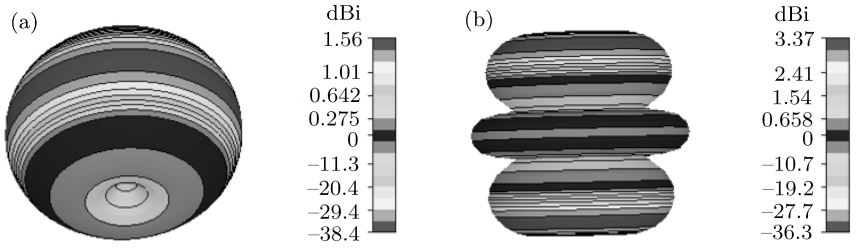


Fig.9. (a) the radiation pattern at 2.47 THz, and (b) at 7.38 THz.

4. Conclusions

To conclude, we have investigated the properties of THz emission from metallic, single walled CNT dipole antenna and have provided a method to generate THz radiation based on CNT. In spite of the low emission power, in comparison with a photoconductor antenna, the CNT antenna attracts much attention and expands the bandwidth of high frequency THz wave. In order to improve the emission power and efficiency, the CNT array has been taken into consideration, which will be described later.

References

[1] Siders C W, Siders J L W, Taylor A J, Park S G, Melloch M R and Weiner A M 1999 *Opt. Lett.* **24** 241
[2] Hu Q L, Liu S B and Li W 2008 *Chin. Phys.* B **17** 1051
[3] Kawase K, Shikata J I and Hiromasa I 2001 *J. Phys.* D: *Appl. Phys.* **35** R1
[4] Sun H Q, Zhao G Z, Zhang C L and Yang G Z 2008 *Acta Phys. Sin.* **57** 790 (in Chinese)
[5] Shi W, Tian L Q, Liu Z, Zhang L Q, Zhang Z Z, Zhou L J, Liu H W and Xie W P 2008 *Appl. Phys. Lett.* **92** 043511-1
[6] Zhang T Y and Zhao W 2008 *Chin. Phys.* B **17** 4285
[7] Shen Y C, Upadhya P C, Linfield E H and Beere H E 2003 *Appl. Phys. Lett.* **83** 3117
[8] Heinze S, Tersoff J, Martel R, Derycke V, Appenzeller J and Avouris Ph 2002 *Phys. Rev. Lett.* **89** 106801
[9] Appenzeller J, Knoch J, Derycke V, Martel, Wind S and Avouris Ph 2002 *Phys. Rev. Lett.* **89** 126801
[10] Wang J and Musameh M 2004 *Analyst* **129** 1
[11] Dresselhaus M S 2004 *Nature* **432** 959
[12] Burke P J, Li S and Yu Z 2006 *IEEE Trans. Nanotech.* **5** 314
[13] Jin H and Hanson G W 2006 *IEEE Trans. Nanotech.* **5** 766
[14] Kempa K, Rybczynski J, Huang Z P, Gregorczyk K, Vidan A, Kimball B, Carlson J, Benham G, Wang Y, Herczynski A and Ren Z F 2007 *Adv. Mater.* **19** 421
[15] Kempa K, Kimball B, Wang Y, Carlson J B, Benham G, Li W Z, Kempa T, Rybczynski J, Herczynski A and Ren Z F 2004 *Appl. Phys. Lett.* **85** 2607
[16] Wang Y, Wu Q, He X J, Sun X F and Gui T L 2008 *Int. J. Infrared Milli. Waves* **29** 35